

Geochronology, geochemistry, and tectonic significance of the Shirensan gneiss in the southern margin of the North China Block

Wang Jingya¹, Ren Shenglian^{1*}, Dong Shuwen², Li Longming¹, Jiang Dazhi³, Shi Yonghong¹, Li Jiahao¹, Song Chuanzhong¹, Han Xu¹, Li Zhenqiang¹, and Ouyang Jue³

¹ HeFei University of Technology, School of Resources and Environmental Engineering, Hefei 230009, China; (migorhappyday@126.com; ren_lotus@126.com)

² Nanjing University, School of Geoscience and Engineering, Nanjing 230026, China

³ Western University, London, School of Earth Sciences, Ontario N6A 3K7, Canada

doi: 10.4154/gc.2019.21



Abstract

The Shirensan Block is a complex geological body located in the southern margin of the North China Block (NCB). From south to north, it can be divided into the Taihua Group migmatite, and the Shirensan gneiss and magmatic rocks. The petrographic features, tectonic setting, provenance, and geological age of the Shirensan gneiss using comprehensive field investigations, microstructural analysis, zircon U-Pb radioactive dating, and geochemical analyses were investigated for this study. The petrology, geochemistry, and geochronology of the Shirensan gneiss suggests that it is mainly a felsic rock and its protolith was a high-K calc-alkaline series A-type granite. The protolith is high in SiO₂, Al₂O₃, K₂O, Na₂O, and low in CaO and MgO. Overall, the Sr-Nd isotope composition of the samples showed no significant difference, indicating that the Taihua Group migmatite and the Shirensan gneiss have the same source material. The Shirensan block may be partially melted from the Taihua group and formed during activity of the Luoluan Fault. By the method of zircon dating analysis, the protolith age of the Shirensan block was determined as 1559±16Ma (Early Proterozoic). Then, the crystallization age of the syntectonic migmatite is 439.2±7.6Ma, which was formed by subduction of the Taihua Group. During the early Cretaceous (119.5±1.3Ma), the Shirensan gneiss may have experienced regional migmatization and formed the zircon rims age of the Yanshanian period. Litho-geochemical features of the Shirensan block are similar to A1-type granites indicating that they are post-orogenic. Therefore, the metamorphic deformation of the Shirensan gneiss reflects the tectonics in the southern margin of the NCB.

Article history:

Manuscript received April 11, 2019

Revised manuscript accepted July 17, 2019

Available online December 20, 2019

Keywords: Qinling Orogenic Belt, North China Block, Shirensan, Geochronology, Geochemistry, Petrology

1. INTRODUCTION

Qinling orogenic belt is a complex subduction-collision orogenic belt that traverses China from east to west (XU et al., 1990, 2015 and Fig. 1). It was formed during several tectonic events and types of activities including subduction, collision, and the intra-continental orogeny of the Yangtze plate and the North China Block (PEI et al., 1995; ZHANG et al., 1997; SONG et al., 2002, 2006). The Qinling orogenic belt can be divided into several tectonic zones including the southern margin of the North China Block, the North Qinling, the South Qinling, and the northern margin of the Yangtze Block, based on its petrology and geotectonic features (ZHANG et al., 2001; DONG et al., 2003; WU et al., 2018). The North China Block has become one of the research hotspots in recent years due to its proximity to the North Qinling, complex, its composition, and multi-stage tectonic evolution.

The Shirensan gneiss (the object of this paper), is located on the southern margin of the North China Block. It coincides with the northern margin of the North Qinling. Previous studies have shown (REN et al., 2013) that it is a product of subduction of the North Qinling beneath the North China Block. Therefore, an in-depth study of the structural geology, petrology, geochemistry, and geochronology of the Shirensan gneiss is of great importance to further current understanding of the interactions between the North Qinling and the southern margin of the North

China Block. Therefore, on the basis of previous studies, comprehensive field petrology and structural geology investigations were undertaken, combined with geochemical and zircon U-Pb chronology, to investigate the tectonic setting and to determine the absolute age of the Shirensan gneiss. The results obtained from this research provide a foundation for further studies on the tectonic evolution of the Mesozoic intracontinental orogeny in the southern margin of the North China Block.

The focus of previous studies in this area was on the genesis and chronology of magmatic rocks. WANG et al. (1988) concluded that the Shirensan gneiss was formed by remelting processes. They also proposed that the Shirensan gneiss was an S-type granite formed by repeated metasomatism-remelting of the Kuanping group schist and gneiss. They suggested that evidence such as the gradual transition between the undeformed granite bodies and the surrounding gneiss, their complex mineralogy and chemical composition supports this idea. ZHANG et al. (1990) concluded that the Shirensan gneiss is a mixed granitic gneiss, which is a progressive granite resulting from the effects of plate collision effect. LU et al. (1995) believed that the leftward horizontal sliding of the Luoluan fault zone was responsible for partial melting and the diapiric uprising of the Taihua group rocks. The partial melt was then intruded into the Taihua group in a “wedge-shape” and deformed together with the Luoluan fault zone to form the granitic gneiss – Shirensan gneiss. Although there have been several research investigations reported on the

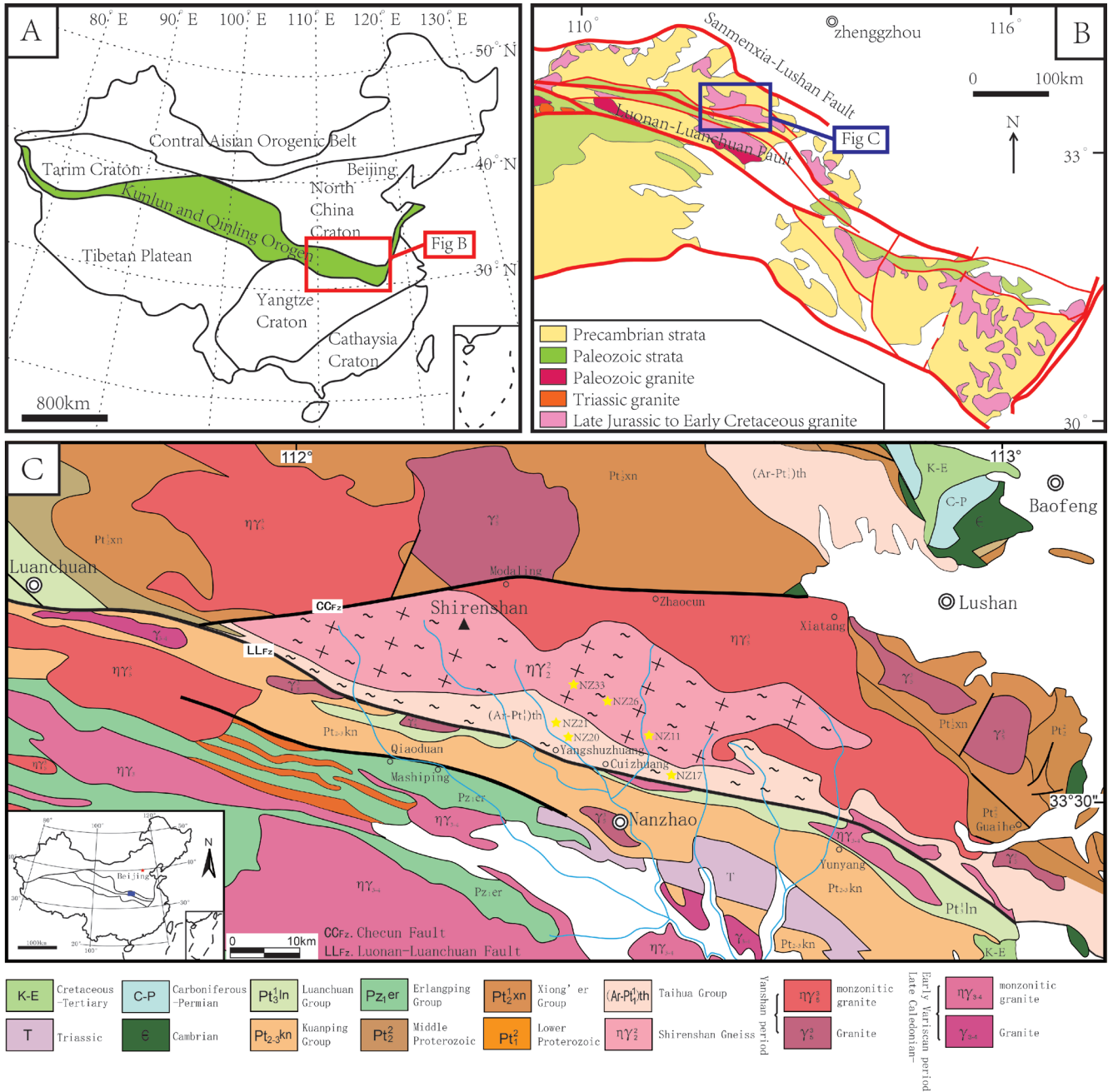


Figure 1. Geological map of the Shirensan block, North Qinling (according to ZHANG et al., 1997).

petrology of the Shirensan gneiss, there is still a lack of understanding of its deformation and tectonic evolution. Hence, the main objective of this research work is to address this issue.

2. GEOLOGICAL SETTING

The Shirensan gneiss is located in Nanzhao County, Henan Province. It is a geological body with characteristic evidence of metamorphic deformation in the Shirensan block of the Luanchuan-Fangcheng section (Fig. 1). The Shirensan block has a surface exposure of about 2000 km² and is structurally controlled by faults. To the north, the Checun fault separates the Shirensan gneiss from the Xiong'er group volcanics. To the south, it is separated from the Kuanping group by the Luonan fault zone.

The Shirensan block consists of granite, Shirensan gneiss and the Taihua group migmatite from north to south, respec-

tively. Except for the northern granite, both the middle part of the Shirensan gneiss and the southern Taihua group migmatite have experienced multiple episodes of strong deformation. They all show evidence of tectonic activities such as subduction, collision, and subsequent intracontinental orogeny in different periods.

3. SAMPLING AND PETROGRAPHIC STUDIES

In order to understand the deformation of the Shirensan gneiss and the Taihua Group migmatite, samples from these two types were collected for petrographic studies.

The Shirensan gneiss samples NZ11, sample NZ26, and NZ33 were collected from the middle of the Shirensan block. They have a medium grain size, platy granitic structure, a gneissic structure, and a local banded and eye-shaped texture. The eyeball structure is composed of flattened and elongated

gray-white plagioclase and light-coloured red plagioclase. The content varies greatly and exhibits obvious preferred orientation. Mylonitization can be commonly observed in the gneiss. The quartz is elongated, similar to a ribbon, and the feldspar is porphyroclastic. The shape of the feldspar has the characteristics of asymmetric organization, illustrating the left-lateral sliding shearing motion.

Sample NZ11 is a felsic gneiss collected from the Nanzhao-Cuhuang section (sampling position coordinates: N33°36'21.06", E112°23'13.8"). It is mainly composed of quartz (50-65 vol %), feldspar (30-35 vol %), mica (10-15 vol %), and amphibole (<1vol %) (Fig. 2a). Quartz is fine-grained in the form of striped single-grains and granular aggregates showing preferred orientation which is an indication of the direction of tectonic movement. Pla-

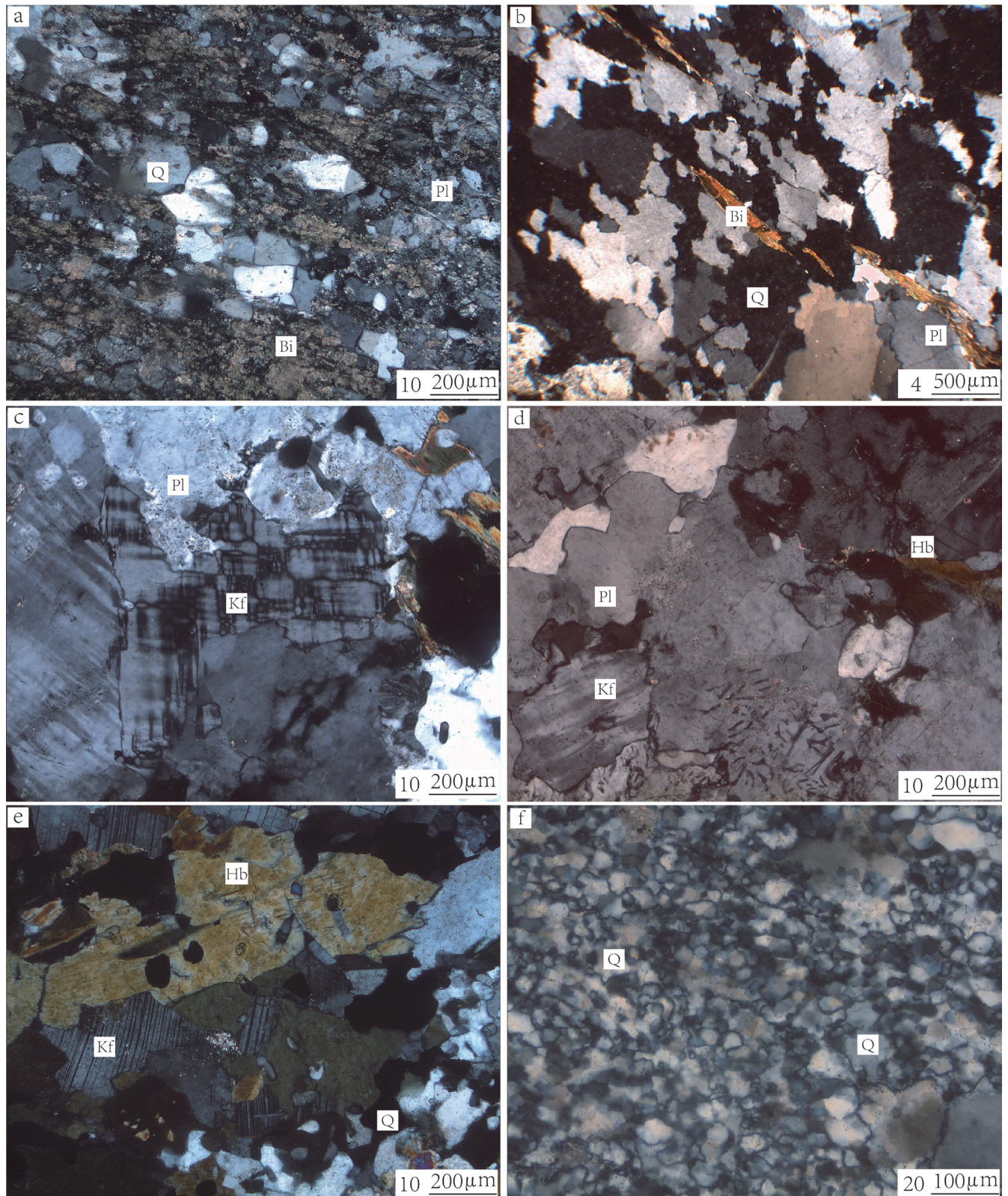


Figure 2. Microstructural features of the samples. (a) NZ-11; (b) NZ-26; (c) NZ-33; (d) NZ-17; (e) NZ-20; (f) NZ-21

gioclase is fresh with polysynthetic twin development. Dark minerals are mainly composed of biotite, which are distributed as fine pieces. They are also sparsely distributed and show preferred orientation and gneissic structure.

Sample NZ26 is a biotite plagiogneiss collected from Liangshichuan (sampling position coordinates: N33°36'18.36", E112°19'48.18"). It is mainly composed of quartz (65-70 vol %), feldspar (35-40 vol %), mica (5-10 vol %), and amphibole (<1 vol %) (Fig. 2b). Part of the feldspar is sericitized and characterized by irregular grain boundaries, wavy and banded extinction, and preferred orientation. Dark minerals are mainly composed of biotite and a small amount of amphibole. The biotite shows a strongly preferred orientation.

Sample NZ33 is a biotite-bearing granitic gneiss, collected from Baichitan, Nanzhao County, Henan Province (sampling location coordinates: N33°39'24.66", E112°17'19.44"). It is mainly composed of quartz (45-50 vol %), feldspar (50-55 vol %), mica (10-15 vol %), and amphibole (<1 vol %) (Fig. 2c). Quartz particles are relatively uniform in size with curved grain boundaries. The feldspar particles are small, dominated by potassium feldspar, with lattice-like twin crystal development, some with sericitization. Dark minerals are mainly composed of amphibole and biotite with obvious preferred orientation and a gneissic structure.

The three rock samples from the Shirensan gneiss are generally from the magmatic rock structure and the minerals did not undergo obvious dynamic recrystallization except for the obvious dynamic recrystallization phenomenon and the mylonite structure in a localised deformation strip. In addition, the dark minerals have obvious orientation, and the microscopic features also show that the dark minerals did not undergo dynamic recrystallization. This indicates that the dark minerals were oriented during the rock crystallization process and are associated with the same tectonic magmatic rock, and the gneiss-like texture is protogenetic.

The Taihua Group migmatite samples NZ17, NZ20, and NZ21 were taken from the Taihua Group located in the south of the Shirensan region. These rocks show a mainly massive structure and are oriented in a northwest-southeast direction. The main rock types include banded migmatites and amphibolite-bearing gneiss, biotite plagiogneiss, and felsic granulite. Quartz grains are all fine-grained, irregular, lenticular, strip-like shape and sub-particle-boundary migration recrystallization. The feldspar is curved crystal faces, and at the side, forming a core mantle structure.

Sample NZ17 is a plagioclase amphibole-bearing gneiss, collected from the Cuizhuang-Cangfang section (sampling position coordinates: N33°35'9.42", E112°22'30.06"). It is mainly composed of quartz (40-45 vol %), feldspar (50-55 vol %), mica (<5 vol %), and amphibole (5-10 vol %) (Fig. 2d). The quartz particles are small and are distributed around a feldspar due to sub-grain dynamic recrystallization. The feldspar crystals are fresh showing polysynthetic twin development and exhibiting plastic deformation characteristics and clear subgranularization. Some of the residual speckles have a core-mantle structure, which shows strong metamorphic deformation. The inner side has a creep deformation structure which is a representative of high temperature. The dark minerals are mainly composed of biotite and hornblende. The biotite is more idiomorphic than the hornblende indicating that it is crystallized later.

Sample NZ20 is a hornblende-bearing felsic gneiss collected from Yangshuzhuang Village, Nanzhao County, Henan Province (sampling location coordinates: N33°35'17.16", E112°19'29.94"). It is mainly composed of quartz (40-45 vol %), feldspar (35-40

vol %), mica (<1 vol %), and amphibole (20-25 vol %) (Fig. 2e). Quartz is strip-shaped, the grain boundary is curved into a leaf shape, and dynamic recrystallization is dominated by boundary migration with a sub-particle form. The feldspar residuals are large, in irregular eyeball shape, with strong wavy extinction, much deformation and cracks. Most of the feldspars are striped with deformation distortion. There are some albite rims around the grains along with some recrystallization at the edges of the granules. The dark mineral is mainly hornblende.

Sample NZ21 is a biotite hornblende-bearing gneiss, collected from Shimiao Bay in Nanzhao County, Henan Province (sampling location coordinates: N33°35'44.88", E112°19'42.6"). It is mainly composed of quartz (30-35 vol %), feldspar (60-65 vol %), mica (5-10 vol %), and amphibole (10-15 vol %) (Fig. 2f). Quartz is with fine granules and signs of strong deformation. All of the minerals exhibit sub-particle-boundary migration recrystallization with strong wavy extinction. The feldspar is in rotating porphyritic form and the ridges are bulged and recrystallized. The biotite is strongly deformed and shows signs of bending and kinking.

In general, the three rock samples from the Taihua Group show strong dynamic recrystallization. This is an indication that they have experienced a certain intensity of tectonic stress after crystallization. From north of the Luoluan fault zone, the grain size of the rocks gradually changes from fine granular, long strips, with strong preferred orientation to coarse-grained and semi-orientated to the granite protolith. The quartz changes from elongate crystals to granular texture, and the recrystallization migrates from sub-particles to the high-temperature boundary. The feldspar gradually changes from fractured and stress textures to subgranulation, with a core-mantle structure and K-metasomatism. These characteristics indicate that under the impact of the Luoluan fault zone, the intensity of deformation inside the Shirensan block gradually weakens from the south Taihua group to the central Shirensan gneiss.

4. ANALYTICAL METHODS

4.1. Zircon dating analysis

The single mineral separation of zircon was completed by the Langfang Laboratory of the Hebei Provincial Geological Prospecting Bureau. After polishing, the optical and cathode fluorescence (CL) of the zircon was observed and the U-Th-Pb isotope analysis was carried out using LA-ICP-MS. The zircon U-Pb dating analysis was completed in the LA-ICPMS Clean Laboratory of the Hefei University of Technology. The laser ablation aperture was 24µm, helium was used as the carrier gas, argon was used as the compensation gas to adjust the sensitivity, and the international standard 91500 was used as the external standard. The NISTSRM610 was selected as the external standard of element content. For every test, 5 samples were selected and tested twice according to standard 91500. The off-line data processing (including selection of sample and blank signals, instrument sensitivity drift correction, element content and U-Th-Pb isotope ratio and age calculation) was performed using the ICPMSDateCal 9.0 software. Detailed instrument operating conditions and data processing methods can be found in the literature (LIU et al., 2010).

4.2. Analysis of major and trace elements

The whole-rock element analysis was carried out in the Australian Minerals Laboratory (Guangzhou) of the Aussie Analytical Testing Group. The main elements were tested by fluorescence spectrometer (XRF), from the Axios instrument produced by PANalytical in the Netherlands. The trace elements were ana-

lyzed by ICP735-ES in the Australian Minerals Laboratory (Guangzhou) of the Aussie Analytical Testing Group. The multi-element content of the rock sample was determined by inductively coupled plasma emission spectroscopy (ICP-AES) after tetracid digestion, and 33 elements were detected (for list of elements see table 2). The alkali fusion method was also adopted for rare earth element (REE) analysis. The rock sample was added to LiBO₂ to be uniformly mixed, melted in a furnace above 1000°C, and 31 elements were detected by inductively coupled plasma mass spectrometry (ICP-MS). The detection instrument used is the Perkin Elmer, USA Production of Elan 9000.

4.3. Whole rock Sr-Nd isotopic analysis

The Sr-Nd isotope separation test of rock samples was completed on the MC-ICP-MS from the laboratory of Nanjing Polypeptide Detection Technology Co., Ltd. The Rb-Sr and Sm-Nd isotope separations of whole rock samples include the process of sample preparation, chemical separation, and testing. The rock powder was dried in an oven and then weighed. Similar to the method of treating samples by ICP-MS, the acid dissolution method was used for the dissolution of the sample. Rb-Sr and Sm-Nd isotope separation was carried out using the conventional cation exchange resin method. The type of resin used for Rb-Sr separation is AG-SOW-X8, and HDEHP resin was used for Sm-Nd separation. For detailed separation and test procedures, see LIU et al. (2004).

5. RESULTS

5.1. Zircon U-Pb age

The zircon crystals of the Shirenshan gneiss are generally 50–150 μm in diameter in the form of elongated grains with an aspect ratio of 2:1~3:1 (Fig. 3). The CL image shows that all zircons have a core-mantle structure. The core is relatively wide, generally larger than 40 μm, with bright luminescence and an obvious magmatic crystallization zone. The rims are narrow, generally less than 10 μm, with very few around 25 μm, with weak luminescence and no obvious structure. The zircon rim and the mantle are rugged, bay-like, jagged, and some dark patches are needle-like or bay-like into the magma core and light core residual can be found in the dark patches which indicate that it is a heterogeneous metamorphic recrystallized structure. The zircon CL structure indicates that the core is part of the magmatic original zircon which was not affected by the metamorphism, and the rim is formed by the later metamorphism episode. The ²⁰⁶Pb/²³⁸U age-weighted average of 11 analysis points from the zircon rims is 119.5±1.3Ma (MSWD=1.5) (Table 1 and Fig. 4a). The ²⁰⁶Pb/²³⁸U age of 9 analysis points from the zircon mantle ranges from 424 to 461 Ma with the weighted mean age of 439.2 ± 7.6 Ma (MSWD = 1.14) (Table 1 and Fig. 4b). In addition, the ²⁰⁶Pb/²³⁸U age of 7 analysis points from the zircon cores is 1506Ma ~ 1592Ma with the weighted average age of 1559±16Ma (Table 1).

Table 1. Zircon U-Pb isotopic data for the samples.

Spot No.	Content (ppm)			Isotopic ratios			Isotopic ages (Ma)		
	Th	U	Pb	²⁰⁷ Pb/ ²⁰⁶ Pb	²⁰⁷ Pb/ ²³⁵ U	²⁰⁶ Pb/ ²³⁸ U	²⁰⁷ Pb/ ²⁰⁶ Pb	²⁰⁷ Pb/ ²³⁵ U	²⁰⁶ Pb/ ²³⁸ U
NZ-1	589	2030	42.96	0.0509	0.1291	0.0183	235	123	117
NZ-2	472	1985	42.76	0.0472	0.1208	0.0184	57.5	116	118
NZ-3	527	3965	81.86	0.0499	0.1282	0.0184	191	122	118
NZ-4	549	2347	49.66	0.0490	0.1257	0.0185	146	120	118
NZ-5	604	1982	46.91	0.0495	0.1318	0.0186	172	126	119
NZ-6	379	2093	45.39	0.0507	0.1325	0.0187	228	126	120
NZ-7	650	2808	60.01	0.0513	0.1335	0.0188	254	127	120
NZ-8	154	1319	27.28	0.0463	0.1217	0.0190	16.8	117	121
NZ-9	553	2112	46.50	0.0506	0.1342	0.0191	220	128	122
NZ-10	363	1730	37.18	0.0499	0.1319	0.0191	191	126	122
NZ-11	154	1208	25.45	0.0532	0.1414	0.0191	339	134	122
NZ-12	204	364	122.4	0.1022	3.7389	0.2631	1665	1580	1506
NZ-13	182	366	124.9	0.0970	3.6212	0.2681	1569	1554	1531
NZ-14	464	691	270.3	0.0959	3.5843	0.2684	1546	1546	1532
NZ-15	181	537	219.7	0.0994	3.6717	0.2728	1613	1565	1555
NZ-16	271	580	197.2	0.0981	3.7342	0.2729	1589	1579	1556
NZ-17	150	204	74.9	0.0973	3.7539	0.2766	1574	1583	1574
NZ-18	360	505	188.4	0.0997	3.9078	0.2801	1618	1615	1592
NZ-19	60.9	678	420	0.0682	0.6413	0.0680	876	503	424
NZ-20	55.0	575	459	0.0544	0.5141	0.0680	387	421	424
NZ-21	29.8	229	243	0.0842	0.8079	0.0698	1298	601	435
NZ-22	17.8	137	181	0.0545	0.5242	0.0699	394	428	436
NZ-23	21.1	147	218	0.0560	0.5445	0.0704	454	441	439
NZ-24	40.7	403	328	0.0549	0.5369	0.0710	409	436	442
NZ-25	29.8	290	221	0.0715	0.7043	0.0719	972	541	447
NZ-26	22.4	106	242	0.0595	0.6009	0.0728	583	478	453
NZ-27	32.0	275	245	0.0727	0.7396	0.0741	1006	562	461

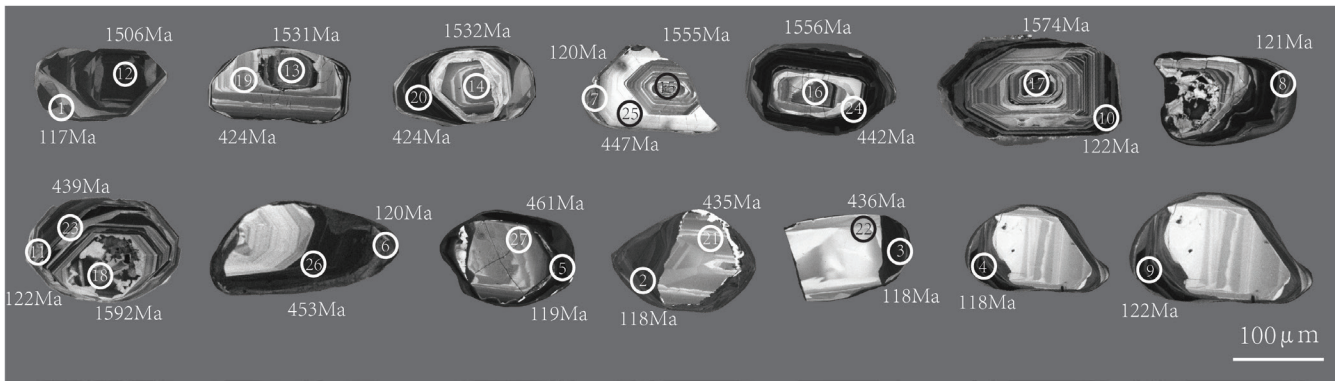


Figure 3. Representative cathodoluminescence (CL) images for zircons from the sample, the open circles are spot analyses with available ²⁰⁶Pb/²³⁸U ages.

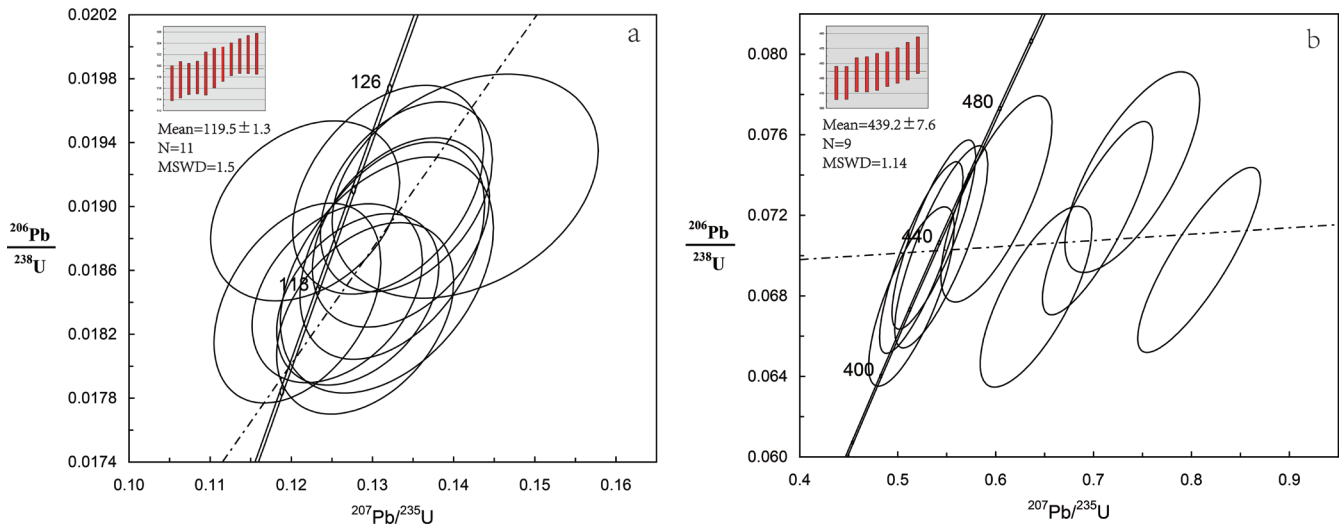


Figure 4. LA-ICP-MS zircon U-Pb isotopic dating. (a) U-Pb isotopic data from the zircon rims and (b) U-Pb isotopic data from the zircon mantles.

5.2. Major elements

A geochemical study of the samples was carried out to shed some light on the provenance of the Shirensan gneiss and the Taihua Group (Table 2). The Shirensan gneiss and Taihua Group migmatites are rich in silica SiO₂ is 69.11-75.43wt%, aluminum Al₂O₃ is 13.41-17.81wt%, and potassium K₂O is 4.05-5.29wt%, with an aluminum saturation index (A/CNK) of 1.37-1.58; which belongs to the high-K calc-alkaline series of strong aluminous granite (Figs. 5, 6). In the Harker diagram (Fig. 7), the contents of TiO₂,

Al₂O₃, MgO, CaO, TFe₂O₃, Na₂O, and P₂O₅ decrease with increasing SiO₂ content showing a good negative linear correlation and indicating that fractional crystallization of sideromelane, plagioclase, and apatite may have played an important role in the process of magma evolution.

The rock is rich in iron and poor in magnesium. The mass fraction of TFe₂O₃ is 1.46-5.24wt% and the mass fraction of MgO is 0.20-1.86wt%. The ratio of TFeO/MgO is 2.54-13.39 (average 6.08 wt%); which is within the range of variation TFeO/MgO in

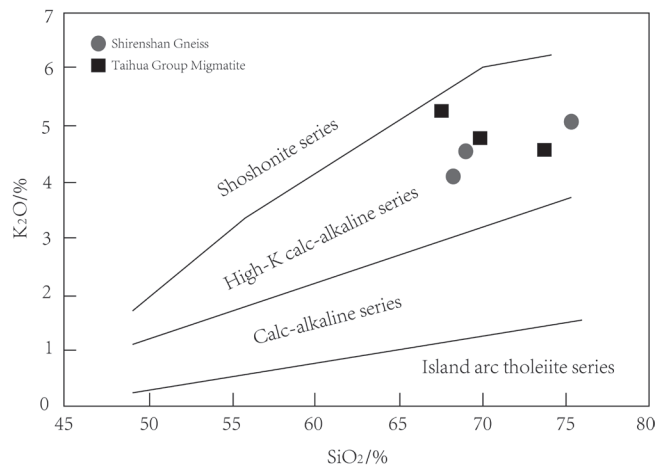


Figure 5. SiO₂-K₂O diagram for the samples (PECCERILLO et al., 1976).

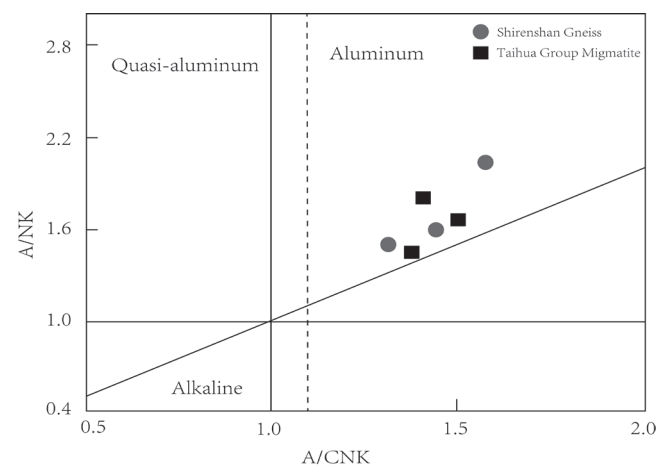


Figure 6. A/CNK-A/NK diagram for the samples (MANIAR et al., 1989).

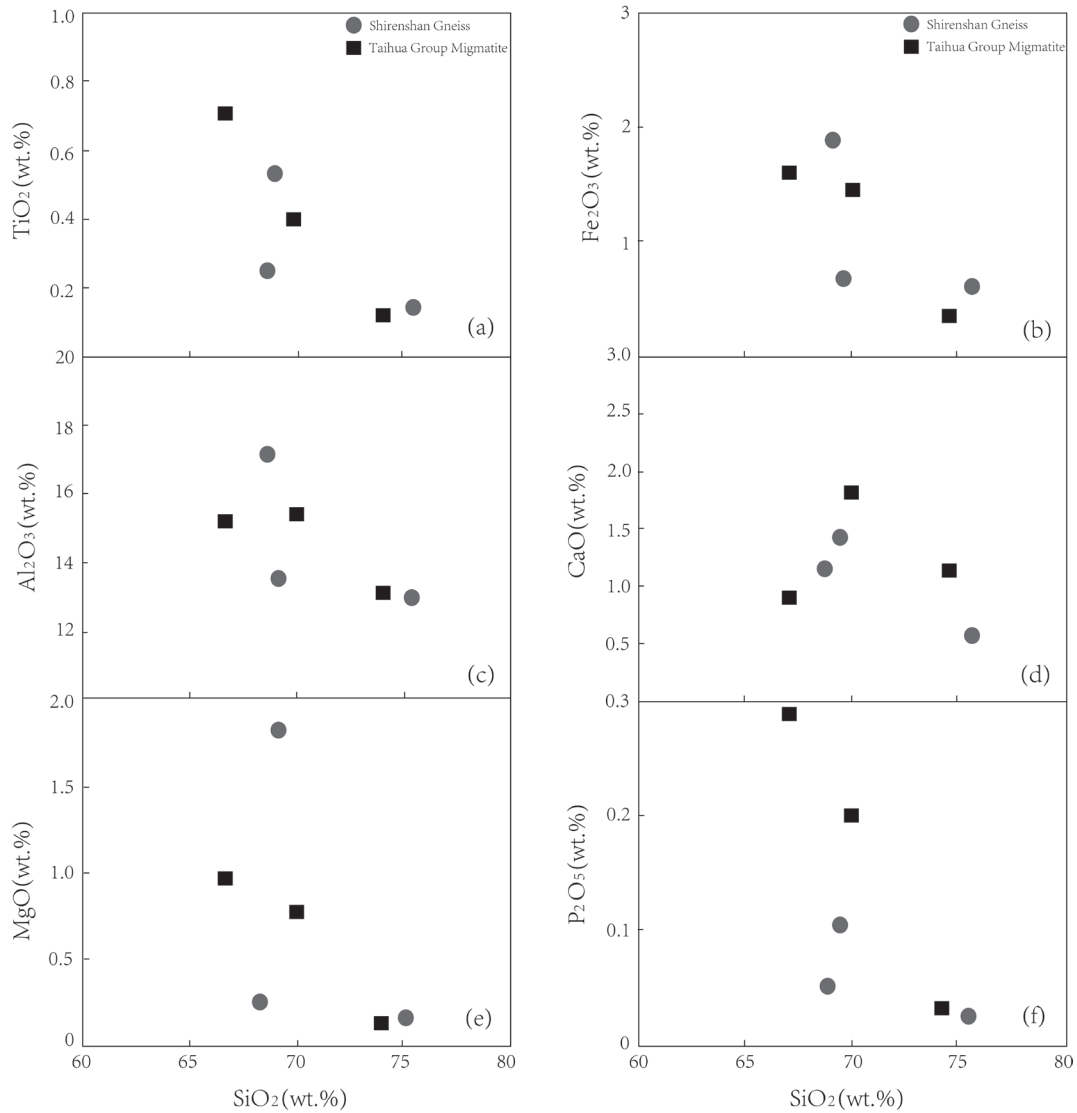


Figure 7. Harker variation diagrams for the samples.

type A granite (KING et al., 1997), and higher than the general I type (the average is 2.27) granite, the S type granite (the average is 2.38) and the M type granite (average 2.37) (King et al., 1997).

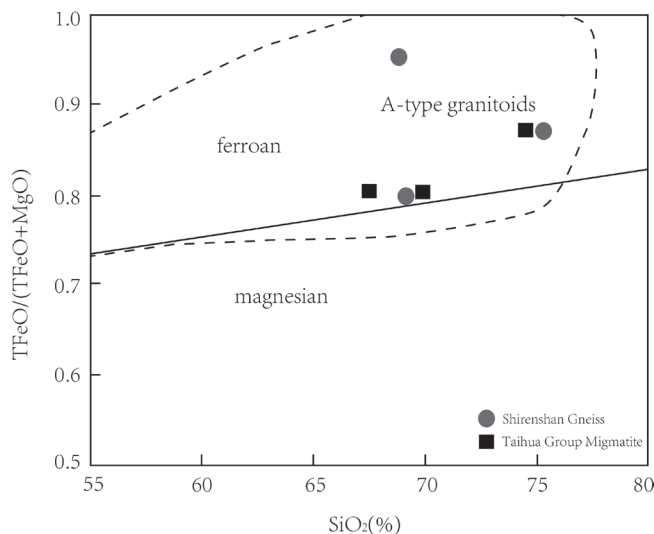


Figure 8. $w(\text{TFeO})/(\text{TFeO}+\text{MgO})-w(\text{SiO}_2)$ diagram for the samples (FROST et al., 2001).

In the $w(\text{TFeO})/(\text{TFeO}+\text{MgO})-w(\text{SiO}_2)$ diagram (Fig. 8), all of the samples fall into the iron region and also the area of A-type granite. From the characteristics of the main elements of the sample, there is no obvious difference between the Shirensan gneiss and the Taihua Group migmatite which indicates that the original rocks of the Shirensan gneiss may come from the Taihua Group.

5.3. Trace and rare earth elements

The total rare earth element (ΣREE) content of the Shirensan gneiss and Taihua group migmatite samples is between 84ppm-230ppm and the content of light rare earth elements is 73ppm-219ppm. The heavy rare earth elements range between 10ppm-25ppm and the ratio of LREE/HREE is 6.41-20.07. Fig. 9a shows the chondrite-normalized rare earth element distribution and the rock generally indicates LREE enrichment, relative to HREE which are depleted.

The ratio of $(\text{La}/\text{Yb})_N$ in the Shirensan gneiss sample is 4.85-10.23 indicating that the light and heavy rare earth elements are highly fractionated. The δEu is also between 0.28 and 0.85 with an average of 0.56 showing a generally V-shaped rare earth element distribution mode with moderate Eu negative anomaly. The mean value of δCe is 0.97 and there is basically no Ce anomaly. The $(\text{La}/\text{Yb})_N$ ratio of the Taihua Group is 35.08-63.42 indi-

Table 2. Main and trace elements geochemical test results for the samples (main elements: wt%; rare earth and trace elements: ppm).

Sample	NZ11	NZ26	NZ33	NZ17	NZ20	NZ21
SiO ₂	69.14	69.11	75.43	67.64	69.36	74.72
TiO ₂	0.57	0.22	0.13	0.78	0.41	0.12
Al ₂ O ₃	13.60	17.81	13.41	15.18	14.94	13.45
TFe ₂ O ₃ (Total of Fe ₂ O ₃)	5.24	4.17	1.65	3.83	2.83	1.46
TFeO (Total of FeO)	4.72	3.75	1.48	3.45	2.55	1.31
MnO	0.09	0.13	0.05	0.09	0.04	0.04
MgO	1.86	0.28	0.22	0.93	0.72	0.20
CaO	1.48	1.07	0.56	0.82	1.76	1.03
Na ₂ O	3.09	7.08	3.70	4.02	3.87	4.06
K ₂ O	4.05	4.84	4.98	5.29	4.87	4.52
P ₂ O ₅	0.11	0.05	0.02	0.28	0.20	0.03
LOI	0.51	0.30	0.36	1.03	0.64	0.67
Total	99.83	100.16	100.59	100.06	99.98	100.40
A/CNK	1.58	1.37	1.45	1.50	1.42	1.40
TFeO/MgO	2.54	13.39	6.73	3.71	3.54	6.55
Na ₂ O/K ₂ O	0.76	1.46	0.74	0.76	0.79	0.90
Ba	590	580	440	780	2060	600
Cr	62	6	15	10	9	13
Hf	6.2	15.8	4.8	4.9	6.2	4.0
Nb	20.7	65.7	39.2	25.6	20.1	27.9
Ga	18.9	21.1	19.0	20.5	20.7	19.4
Rb	210	122.0	280	120.5	127.0	191.5
Sr	187.0	193.5	120.0	240	850	175.0
Ta	1.7	2.5	5.3	1.9	2.3	2.2
Th	0.88	0.47	0.97	0.82	0.57	0.45
U	5.18	0.71	14.85	2.00	4.39	5.41
Y	29.1	13.8	38.8	24.5	14.4	19.4
Zr	230	837	131	184	227	111
La	44.8	16.2	40.8	40.1	50.4	28.9
Ce	83.8	39.2	75.7	84.2	107.0	53.7
Pr	8.97	4.90	7.91	9.61	11.50	5.19
Nd	34.1	20.0	27.9	37.8	42.1	17.2
Sm	6.37	3.77	5.30	6.36	6.88	3.01
Eu	3.15	1.64	4.29	2.25	1.30	2.11
Gd	5.80	3.18	5.46	5.80	4.61	2.77
Tb	0.88	0.47	0.97	0.82	0.57	0.45
Dy	5.40	2.78	6.48	4.66	3.02	3.14
Ho	1.05	0.54	1.31	0.87	0.51	0.66
Er	3.15	1.64	4.29	2.25	1.30	2.11
Tm	0.48	0.28	0.71	0.32	0.18	0.35
Yb	3.12	1.85	4.72	1.92	1.18	2.46
Lu	0.51	0.33	0.80	0.29	0.17	0.40
Y	29.1	13.8	38.8	24.5	14.4	19.4
LREE	178.68	73.06	158.51	179.7	219.3	108.5
HREE	20.39	11.07	24.74	15.83	10.93	10.33
LREE/HREE	8.76	6.60	6.41	11.35	20.07	10.50
ΣREE	199.07	84.13	183.25	195.6	230.3	118.8
(La/Yb) _N	10.23	4.85	6.25	35.08	63.42	46.07
Eu/Eu*	0.56	0.85	0.28	0.82	0.74	0.47
Ce/Ce*	0.97	0.97	0.97	1.02	1.05	0.99

cating that the fractionation of light and heavy rare earth elements is weak. The Eu of the rock samples shows an evident negative anomaly, and the Eu/Eu* is between 0.47-0.82.

Figure 9b illustrates the primitive mantle standardized trace element spider diagram, where the Shirensan gneiss and Taihua group migmatites are rich in Cs, Rb, Th, U, La, and other large

ion lithophile elements and high field strength elements Nb, Ta, Zr, and Hf. They are also very poor in Sr, P, Ti, and other elements; which, is different from arc magmas. Compared to the Taihua Group migmatite, the Shirensan gneiss is richer in Th, U, Zr, and Hf, and depleted in Ba, Ce, and Y where P and Sr are negative anomalies indicating the presence of plagioclase in the rock as a

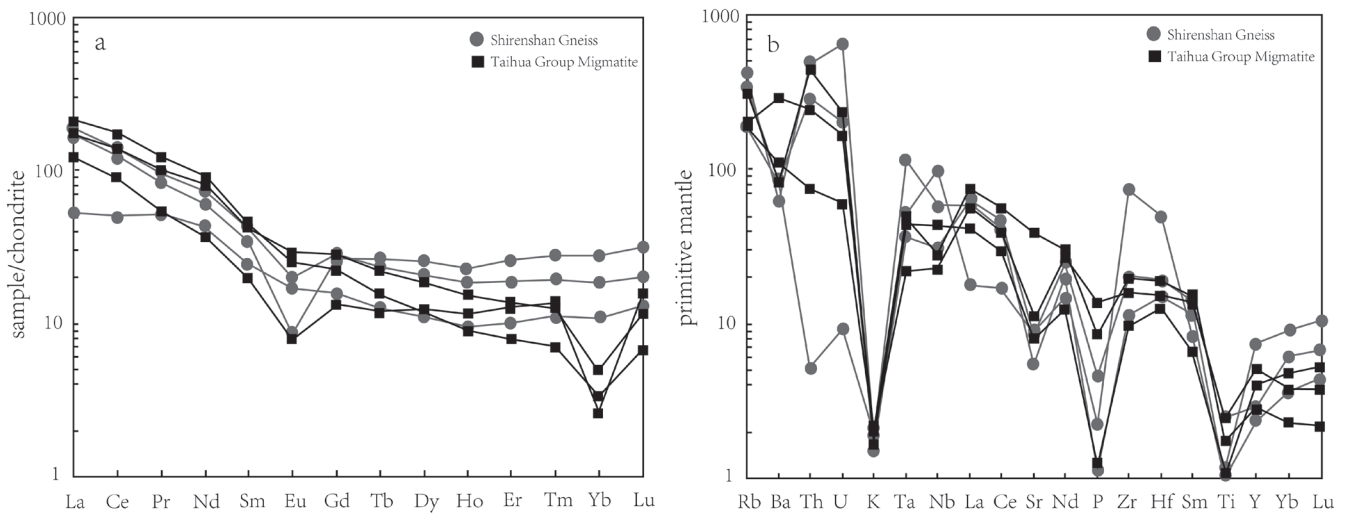


Figure 9. (a) Chondrite normalized REE patterns and (b) primitive mantle normalized trace element diagrams. (Normalization values after SUN et al., 1989).

molten residual phase or a crystalline separation phase. This supports a close relationship between the source rock material of the Shirensan gneiss and the continental crust (SYLVESTER, 1998). The large losses of P and Ti indicate that the magma has undergone crystallization and separation of secondary minerals such as apatite and rutile (ROBERTS, 1993). In addition, the Rb/Sr ratio of the Shirensan gneiss and Taihua Group migmatite samples is higher than the Rb/Sr ratio of the crust (0.25), indicating that the source rock material may have an argillaceous crustal protolith (SISSON, 2005). In general, the Shirensan gneiss and Taihua group migmatite samples show similar curve characteristics indicating that trace elements have similar geochemical behaviour and common source region properties.

5.4. Sr-Nd isotope

In this paper, six samples from the Shirensan gneiss and Taihua Group migmatite were selected for Sr-Nd isotope analysis (Table 3). There is no significant difference between the Sr-Nd isotopic compositions of the Taihua Group migmatite and the Shirensan gneiss samples. Among the Shirensan gneiss samples, $(^{87}\text{Sr}/^{86}\text{Sr})_i=0.71158\text{--}0.71763$, $\varepsilon_{\text{Sr}}(t)=61.9\text{--}62.4$, $(^{143}\text{Nd}/^{144}\text{Nd})_i=0.511688\text{--}0.5122124$, $\varepsilon_{\text{Nd}}(t)=-6.3\text{--}6.0$, among the Taihua group migmatite samples, $(^{87}\text{Sr}/^{86}\text{Sr})_i=0.71193\text{--}0.71751$, $\varepsilon_{\text{Sr}}(t)=61.8\text{--}62.2$, $(^{143}\text{Nd}/^{144}\text{Nd})_i=0.5116956\text{--}0.5123385$, $\varepsilon_{\text{Nd}}(t)=-5.9\text{--}5.5$.

6. DISCUSSION

6.1. Geochronological significance

In order to define the ages of multiple tectonic activity, LA-ICP-MS zircon U-Pb dating was performed on the Shirensan gneiss and the weighted average age of $^{206}\text{Pb}/^{238}\text{U}$ was obtained; $119.5\pm 1.3\text{Ma}$ and $439.2\pm 7.6\text{Ma}$. Some of the zircon cores are older

and have a weighted average age of $1559\pm 16\text{Ma}$ which represents the age of the intact rock without complete melting. It can be seen from the mineralogical characteristics and zircon age determinations (Table 1) that the zircon core of the Shirensan gneiss was formed during the Mesoproterozoic. This is similar to the age of the Taihua Group (GAO et al., 2014) and indicates that the zircons of the Shirensan gneiss originated from the ancient Taihua group. Zircon metamorphism is relatively low and the characteristics of magma crystallization are preserved. The age of $439.2\pm 7.6\text{Ma}$ in the mantle is the crystallization age of the magma after melting, which is consistent with the age of subduction of the Luoluan fault zone in the south of the Taihua Group gneiss (REN et al., 2016). This can be attributed to partial melting of the Taihua Group resulting from subduction and shearing of the Luoluan fault zone in the south of the Taihua Group. The age of the zircon rim of $119.5\pm 1.3\text{Ma}$ corresponds to the intrusive age of the undeformed granite on the north side of the Shirensan gneiss (WANG et al., 2017). In the Yanshanian period, due to regional migmatization, undeformed granite of Yanshanian age invaded the north side.

These results together with previous research data (REN et al., 2013) suggest that the Shirensan gneiss protolith may have originated from the ancient geological bodies around the southern margin of the North China Block. Subduction of Luoluan fault zone from the south to the north in the late Caledonian particularly caused partial melting of the Taihua Group on the upper plate, and then invaded the weak zone caused by the left-lateral sliding leading to the formation of homotectonic magmatic rocks. The left-lateral sliding during the plastic phase resulted in the formation of the primary surface. After the crystallization of the magma, the left-lateral sliding activity continued and formed a mylonite strip in the gneiss. During the early Cretaceous period,

Table 3. Sr-Nd isotope data for the samples.

Sample	NZ11	NZ26	NZ33	NZ17	NZ20	NZ21
$87\text{Sr}/86\text{Sr}$	0.711608	0.715894	0.717684	0.711963	0.715518	0.717557
$(87\text{Sr}/86\text{Sr})_i$	0.71158	0.71586	0.71763	0.71193	0.71555	0.71751
$\varepsilon_{\text{Sr}}(t)$	61.9	62.3	62.4	61.9	62.2	61.8
$143\text{Nd}/144\text{Nd}$	0.511759	0.5117169	0.5122322	0.5120851	0.5123903	0.5117765
$(143\text{Nd}/144\text{Nd})_i$	0.511703	0.511688	0.5122124	0.512064	0.5123385	0.5116956
$\varepsilon_{\text{Nd}}(t)$	-6.0	-6.3	-6.1	-5.6	-5.5	-5.9

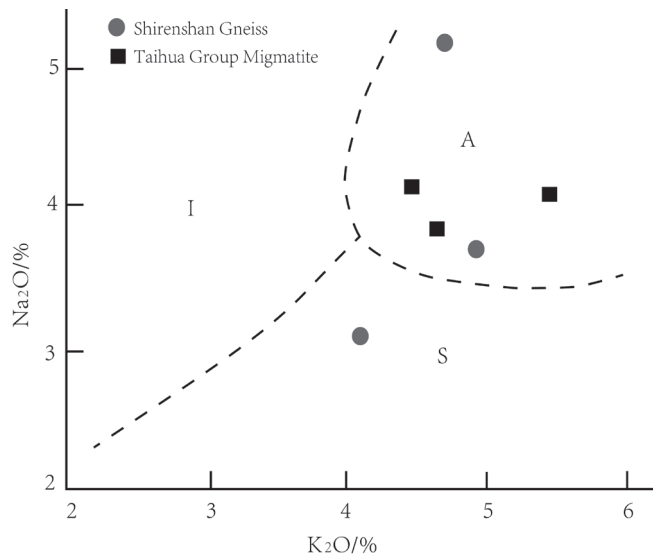


Figure 10. Na₂O-K₂O diagram of the samples, legend A, I, S type granite (COLLINS et al., 1982).

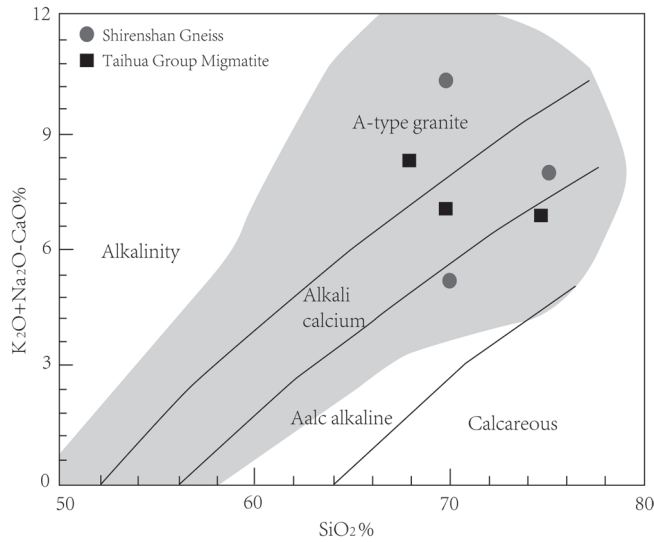
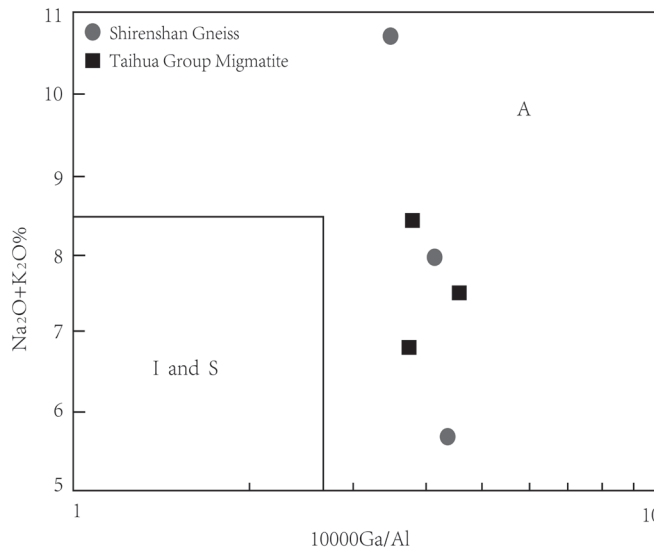


Figure 11. (Na₂O + K₂O - CaO) - SiO₂ diagram of the samples (FROST et al., 2001).



due to regional migmatization, a large number of undeformed granites intruded into the northern part of the Shirenschan gneiss and experienced extensive thermal transformation.

6.2. Precursor of the Shirenschan gneiss

PITCHER (1982) classified granites into four types (I, S, M, and A) based on their differences in protolith and geochemical properties. This classification has been widely applied in the research on petrogenesis (COLTISS et al., 1982; WHALEN et al., 1987; EBY, 1990). The M-type granite parental magma is derived from subducted oceanic crust or mantle wedge melting. After extensive fractional crystallization, a series of continuous gabbro and diorite rock combinations (PITCHER, 1982) were formed with geochemical properties of low Rb, Zr, Nb, Y, and REE content (WHALEN et al., 1987). Since A/CNK<1 and this characteristic is not consistent with the characteristics of the Shirenschan gneiss, the protolith is highly unlikely to be an M-type granite. The S-type granite source rocks are dominated by Al-rich sedimentary rocks. Al supersaturation and the minerals cordierite and muscovite often occur. Alternatively, S-type granites generally have lower oxygen fugacity, Fe³⁺/(Fe³⁺+Fe²⁺) is about 0.153 (CHAPPELL, 1999). There is no aluminium-rich mineral production in the Shirenschan gneiss and the mean value of Fe³⁺/(Fe³⁺+Fe²⁺) is 0.53. This is obviously different from that of S-type granites. The sample shows a peraluminous feature, A/CNK>1.1, ⁸⁷Sr/⁸⁶Sr>0.705, which is not inconsistent with the geochemical characteristics of type I granites. The Shirenschan gneiss has the characteristics of high silicon (SiO₂ content > 67.64), alkali-rich ((Na₂O+K₂O) content > 7.14%), calcium-poor (CaO content < 2.87%), and high FeO^T/MgO ratio (>3.5). The sample data points in the Na₂O-K₂O diagram (Fig. 10) fall into the A-type granite range. Furthermore, the rock is relatively rich in REE (except Eu) and the large ion lithophile elements (Cs, Rb, Th, U, La). However it is very poor in Nb, Ti, and Hf and the other high field strength elements with a high 10000Ga/Al ratio >2.6, (the lower limit of the A-type granite is 2.6). These features show that the Shirenschan gneiss originated from a A-type granite (Figs. 11 & 12).

Type A granites are a product of post-collision or an intra-plate environment. According to their geochemical characteristics, type A granites can be further divided into two subtypes, A1 and A2 (EBY, 1992). The A1 type granite generally represents

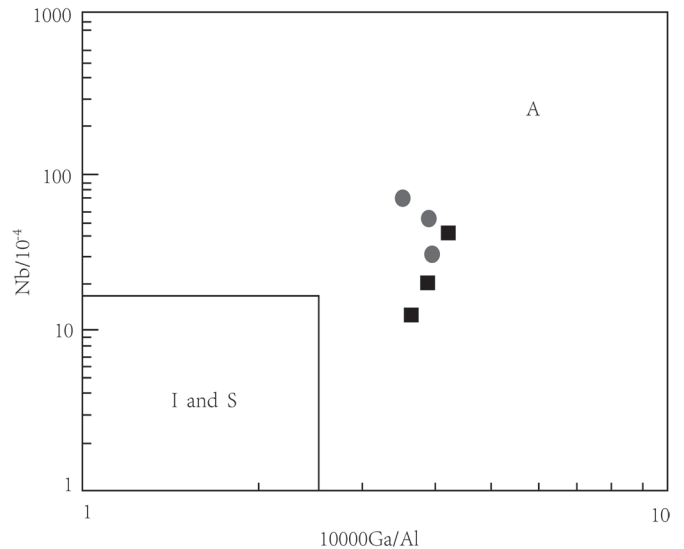


Figure 12. Na₂O + K₂O and Nb-10000Ga/Al diagram of the samples (WHALEN et al., 1987).

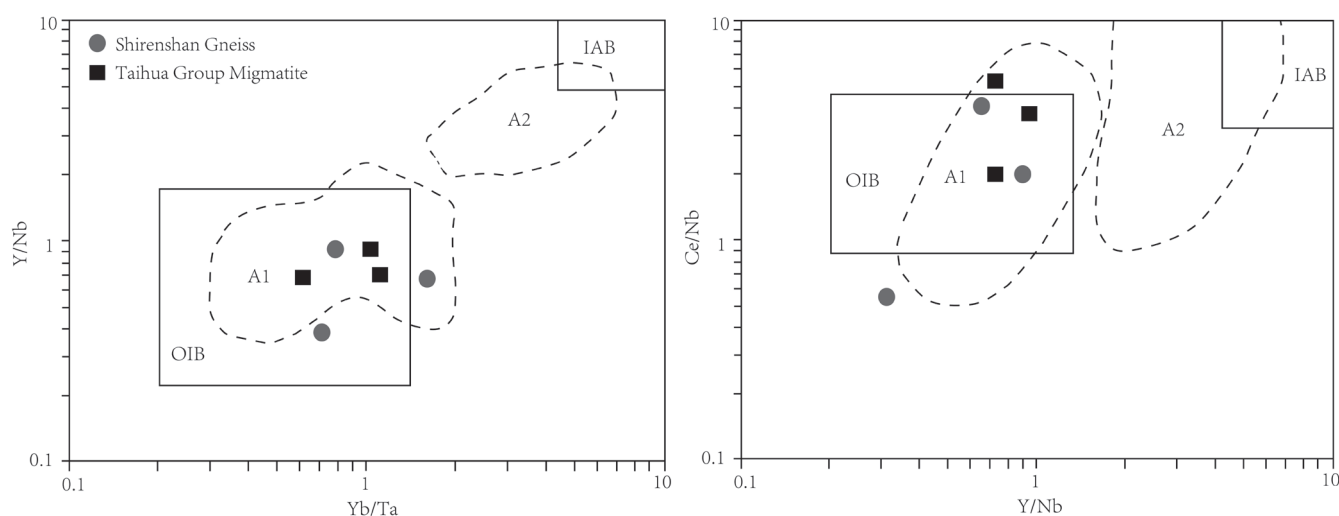


Figure 13. Y/Nb-Yb/Ta and Ce/Nb-Y/Nb diagrams (EBY, 1992).

a non-orogenic continental rift or intraplate environment. An A1 type granite source area is similar to the source area of the ocean island basalt (OIB) intruding into the continental rift under the non-orogenic system or the tectonic setting related to the mantle plume and hotspot. The source rock of the A2 type granite originates from the continental crust or crust formed during underplating in a continent-continent collision or island arc environment and its characteristic element ratio is between the island arc basalt (IAB) and the average continental crust (EBY, 1992). Since the ratio of Y/Nb and Yb/Ta is mainly controlled by the rock type in the source area, the crystallization differentiation of pyroxene, hornblende, and opaque minerals has a weak influence on the above ratio, the ratio of Y/Nb and Yb/Ta can be used to distinguish between the two types of A-type granites (EBY, 1992). In the Y/Nb-Yb/Ta and Ce/Nb-Y/Nb discriminant diagrams, the sample basically falls into the A1 type granite area (Fig. 13). It can be concluded here that the Shirensan gneiss has a geochemical signature of an A1 type granite.

6.3. Material source and genetic model

The following genetic mechanisms were proposed in the literature for the formation of A-type granites: (1) partial melting of crustal materials at low pressure and high temperature (COLLINS et al., 1982; WHALEN et al., 1987; DOUCE, 1995); (2) direct derivation from the mantle source alkali basaltic magma (EBY, 1992; TURNER et al., 1992); and (3) a mixed product of the mantle source alkali basaltic magma and the magma formed under crust source anatexis (MINGRAM et al., 2000; BONIN, 2004).

Since the Y-Yb incompatibility is stronger than the Nb and Ta, the magma formed by the partial melting of the lower crust or the upper crust has a higher Yb/Ta and Y/Nb ratio than the lower crust or the upper crust (RUDNICK et al., 2003). The ratio

of the above elements in the Shirensan gneiss is significantly lower than the ratio of the crust indicating that the genetic mechanism of partial melting of crustal material can be ruled out.

Previous studies have also shown that type A granite can be formed directly by fractional crystallization of mantle source basaltic magma (TURNER et al., 1992; DOUCE, 1995; KING et al., 1997). The intermediate-acid intrusive rocks with the same age as the Shirensan gneiss such as the Taishanmiao granite and the Funiu Mountain granite, are common at the southern margin of the North China Block (REN et al., 2013). These rocks are often rich in Rb, Ba, and Sr, large ion lithophile elements and high field strength elements such as Nb, Ta, Zr, and Hf, and relatively low in Nd isotopes, derived from the OIB melt formed by the asthenosphere metasomatized lithospheric mantle (WANG et al., 2019). The Shirensan gneiss is enriched with light rare earth elements, large ion lithophile elements, and high field strength elements. This is consistent with the basalt formed from the asthenosphere metasomatized lithospheric mantle (TURNER et al., 1992). Hence, it is speculated that the Shirensan gneiss may have a close genetic relationship with the mantle-derived magma at that time.

In general, crustal contamination can result in the loss of Nb and Ta in the magma, the enrichment of Pb, and also affect the composition of the Sr, Nd, and Hf isotopes in the rock (RUDNICK et al., 2003). According to GAO et al. (2014), zircons in the gneiss in the Shirensan area have a negative $\epsilon_{\text{Hf}}(t)$ value (Table 4), a relatively discrete age distribution, and relatively enriched Pb elements. This shows that the magma has undergone a degree of crustal contamination during the upwelling process. However, there is no loss of Nb and Ta in the Shirensan gneiss, which may be related to the relatively high concentration of high field strength elements and relatively weak crustal contamination in the rock source area.

Table 4. LA-MC-ICP-MS zircon Hf isotope data of the Shirensan gneiss (according to GAO et al., 2014).

Spot	$^{176}\text{Yb}/^{177}\text{Hf}$	$^{176}\text{Lu}/^{177}\text{Hf}$	$^{176}\text{Hf}/^{177}\text{Hf}$	$\epsilon_{\text{Hf}}(t)$	$T_{\text{DM1}}(\text{Ma})$	TC DM	$f_{\text{Lu/Hf}}$
No.1	0.013499	0.000608	0.281904	-27.9	1877	2930	-0.98
No.2	0.024122	0.001022	0.282429	-9.4	1165	1777	-0.97
No.3	0.032895	0.001364	0.282356	-12.0	1279	1942	-0.96
No.4	0.030050	0.001279	0.282241	-12.8	1309	1993	-0.96
No.5	0.012840	0.000612	0.282394	-15.9	1412	2190	-0.98
No.6	0.009096	0.0011124	0.282262	-10.6	1379	1856	-0.97

Based on the above analysis, it can be concluded that the Shirensan gneiss was formed from the asthenosphere metasomatized lithospheric mantle during fractional crystallization. In addition, this set of OIB-like melts were affected by a degree of crustal contamination during the magma emplacement process.

6.4. Geodynamic setting

Type A granites have special petrogenetic significance and are only produced in a specific tectonic setting. The formation of A2 type granite is completed in a continent-continent collision environment or related to island arc magmatism; while the formation of A1 type granite occurs in a non-orogenic environment such as a continental fracture or inner plate related to an extension system (EBY, 1992). The Shirensan gneiss in this study is an A1 type granite formed at 439 Ma. Its source area is similar to an oceanic island environment signature and is related to the Taihua Group migmatite. As shown in Fig.15, the sample points all fall into the area of granite at the plate. The previous studies concluded that this type of magmatic activity is often associated with mantle plume or asthenosphere mantle upwelling (EBY, 1992). The existing geological data indicates that the southern margin of the North China Block was outwith the non-supercontinent and an ancient oceanic basin developed at the margin (CAWOOD et al., 2013). In addition, there are no continental flood basalts in the North Qinling Block. It can be concluded here that the Shirensan gneiss is highly unlikely to be associated with mantle plume activity.

The fracture zone of the subduction plate leads to back-arc extension and crustal thinning which can induce upwelling of the hot asthenospheric mantle forming a magma similar to OIB. For example: the eastern Alps (QORBANI et al., 2015), Mediterranean region (JOLOVET et al., 2015), and Central Mexico (FERRARI, 2004). Hence, we suggest that the Shirensan gneiss was formed in the following dynamic setting: prior to formation of the Shirensan gneiss, the southern margin of the North China Block was in a subduction-related island arc environment. The widely exposed Shirensan gneiss is an A1 type granite and was formed in a back-arc extension environment. The geochemical characteristics of the Shirensan gneiss are similar to the geochemical characteristics of the magmatic rocks formed in relation to the fracture zone of the subduction plate in both China and around the world. Both are rich in large ion lithophile elements Rb, K, U, and Pb and high field strength (HFS) elements Nb, Ta, Zr, and Hf from the asthenosphere metasomatized lithospheric

mantle. Due to the similarity of the Sr-Nd isotope composition of the Shirensan gneiss and the Taihua Group migmatite, the geochemical characteristics of the main trace elements are inherited. This indicates that the Taihua Group rock has the same material source as the gneiss in the middle of the Shirensan area.

Based on the above regional geological data and previous research, the authors believe that at the southern margin of the North China Block, subduction and the strike-slip Luoluan fault zone resulted in crustal thinning, asthenosphere mantle upwelling, partial melting of the Taihua Group rocks, and the formation of a syntectonic magma during the Late Caledonian period. Beneath the subduction plate fault system, the intrusive fault zone along the tectonically weak zone facilitated the gneiss formation. During the early Cretaceous period, due to regional migmatization, a large number of undeformed granites intruded the north side resulting in the Yanshanian age. Hence, the metamorphic deformation of the Shirensan gneiss is a reflection of the tectonic-magmatic activity in the Shirensan area on the southern margin of the North China Block. This is of great significance for further studies on the plate edge deformation during the subduction process.

7. CONCLUSIONS

Through a detailed study of structural geology, petrology, geochemistry, chronology, and tectonic environment of the Shirensan gneiss, the following conclusions can be drawn:

(1) The protolith age of the Shirensan gneiss is 1559 ± 16 Ma (early Mesoproterozoic). Then, it was melted under the impact of the subduction of the plate and formed an isostructure magmatite with a crystallization age of 439.2 ± 7.6 Ma (Late Caledonian). At 119.5 ± 1.3 Ma, the early Cretaceous, the Shirensan gneiss may have undergone regional migmatization which results in the age of the Yanshanian.

(2) The Shirensan gneiss is mainly composed of biotite plagiogneiss and felsic gneiss characterized by its high SiO_2 , Al_2O_3 , K_2O , Na_2O , and low CaO, MgO. It is a strong peraluminous high-K calc-alkaline A1 granite formed in an oceanic island environment molded by the asthenosphere metasomatized lithospheric mantle under fractional crystallization with a degree of crustal contamination.

(3) There is no significant difference in the main trace elements and Sr-Nd isotopic compositions of the samples. This indicates that the Taihua Group migmatite and the Shirensan gneiss have the same material source, namely the Shirensan

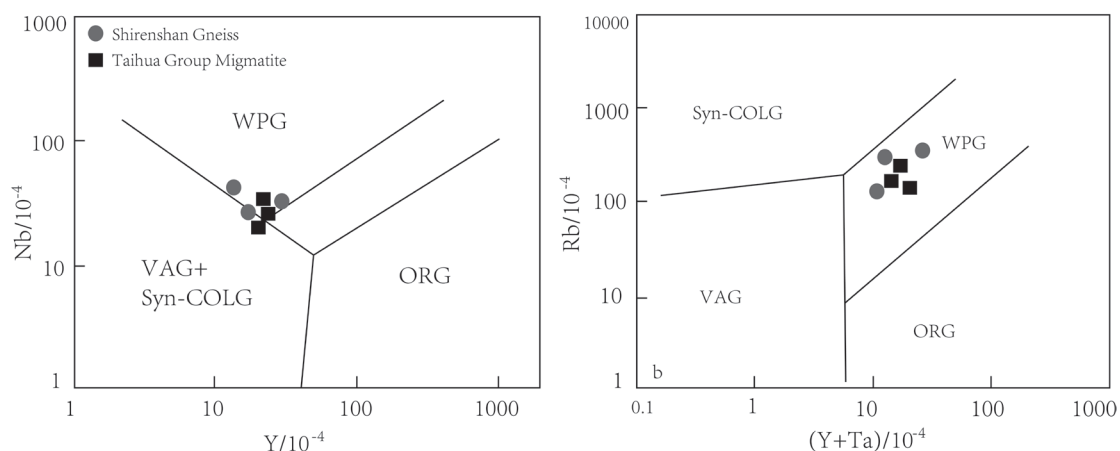


Figure 14. A granitic gneiss tectonic discrimination map. Legend: volcanic arc granite (VAG), syn-tectonic collision granite (Syn-COLG), within plate granite (WPG) and ocean ridge granite (ORG) (PEARCE et al., 1984).

block. Gneiss may be formed due to partial melting of the Taihua Group and deformation of the Luoluan fault zone.

(4) Combining regional tectonic evolution characteristics and geochemical characteristics of the Shirensan gneiss, the authors believe that the Shirensan gneiss in the southern margin of the North China Block has the structural properties of an intraplate granite. This suggests that during the Late Caledonian period, the southern margin of the North China Block was in a back-arc extension environment caused by the rupture of the subducting slab.

ACKNOWLEDGEMENT

This study was supported by the National Nature Science Foundation of China (Nos. 41572177, 41272213, 41573023, 41072161, 41502193, 41272222). The authors wish to express their gratitude to the reviewers for their thoughtful suggestions and comments. Thanks are also due to all who have contributed to the execution of this research.

REFERENCES

- BONIN, B. (2004). Do coeval mafic and felsic magmas in postcollisional to within-Plate regimes necessarily imply two contrasting, mantle and crustal, sources? A review. – *Lithos*, 78/1, 1–24. doi: 10.1016/j.lithos.2004.04.042
- CAWOOD, P. A., WANG, Y. J. & XU, Y. J. (2013). Locating South China in Rodina and Gondwana: A Fragment of Greater India Lithosphere? – *Geology*, 41/8, 903–906. doi: 10.1130/G34395.1
- CHAPPELL, B. (1999). Aluminium saturation in I and S-type granites and the characterization of fractionated haplogranites. – *Lithos*, 46/3, 535–551. doi: 10.1016/S0024-4937(98)00086-3
- COLLINS, W.J. (1982). Nature and origin of A type granites with particular reference to Southeastern Australian. – *Contributions to Mineralogy and Petrology*, 80/6, 189–200.
- DONG, Y.P., ZHANG, G.W. & ZHAO, X. (2003). The proterozoic tectonic framework and evolution of the north Qinling orogen, central China. (in Chinese, with an English Abstract). – *Geotectonica et Metallogenia*, 27/2, 115–124.
- DOUCE, A.E.P. & BEARD, J.S. (1995). Dehydration-melting of biotite gneiss and quartz amphibolite from 3 to 15 kbar. – *Journal of Petrology*, 36/3, 707–738. doi: 10.1093/ptrology/36.3.707
- EBY, G.N. (1990). The A-type granitoids: A review of their occurrence and chemical characteristics and speculations on their petrogenesis. – *Lithos*, 26/1–2, 115–134. doi: 10.1016/0024-4937(90)90043-Z
- EBY, G.N. (1992). Chemical subdivision of the A-type granitoids: Petrogenetic and tectonic implication. – *Geology*, 20/7, 641–644. doi: 10.1130/0091-7613(1992)020<0641:CSOTAT>2.3.CO;2
- FERRAR, L. (2004). Slab detachment control on mafic volcanic pulse and mantle heterogeneity in Central Mexico. – *Geology*, 32/1, 77. doi: 10.1130/G19887.1
- FROST, B.R., BARNES, C.G., COLLINS, W.J., ARCULUS, R.J., ELLIS, D.J. & FROST, C.D. (2001). A geochemical classification for granitic rocks. – *Journal of Petrology*, 42/11, 2033–2048. doi: 10.1093/ptrology/42.11.2033
- GAO, X.Y., ZHAO, T.P. & CHEN, W.T. (2014). Petrogenesis of the early Cretaceous Funiushan granites on the southern margin of the North China Craton: Implications for the Mesozoic geological evolution. – *Journal of Asian Earth Sciences*, 94/2014, 28–44. doi: 10.1016/j.jseas.2014.07.042
- JOLIVET, L., MENANT, A. & STERNAI, P. (2015). The geological signature of a slab tear below the Aegean. – *Tectonophysics*, 659, 166–182. doi: 10.1016/j.tecto.2015.08.004
- KING, P.L., WHITE, A.J.R. & CHAPPELL, B. W. (1997). Characterization and origin of Aluminous A-Type Granites from the Lachlan Fold Belt, Southeastern Australia. – *Journal of Petrology*, 38/3, 371–391. doi: 10.1093/ptrology/38.3.371
- LIU, Y.S., GAO, S., YUAN, H.L., ZHOU, L., LIU, X.M., WANG, X.C., HI, Z.C. & WANG, L.S. (2004). U/Pb zircon ages and Nd, Sr and Pb isotopes of lower crustal xenoliths from North China Craton: Insights on evolution of lower continental crust. – *Chemical Geology*, 211/1–2, 87–109. doi: 10.1016/j.chemgeo.2004.06.023
- LIU, Y.S., HU, Z.C., ZONG, K.Q., CAO, C.G., CAO, S., XU, J. & CHEN, H.H. (2010). Reappraisal and refinement of zircon U-Pb isotope and trace element analyses by LA-ICP-MS. (in Chinese, with an English Abstract). – *Chinese Science Bulletin*, 55/15, 1535–1546.
- LU, S.W. (1995). Geological characteristics of granite in Funiushan region and its genesis. (in Chinese, with an English Abstract). – *Henan Geology*, 13/3, 183–190.
- MANIAR, P.D. & PICCOLOLI, P.M. (1989). Tectonic discrimination of granitoids. – *Geological Society of America Bulletin*, 101/5, 635–643. doi: 10.1130/0016-7606(1989)101<635:TD0G>3E2.3.CO;2
- MINGRAM, B., TRUMBULL, R. B. & LITTMAN, S. (2000). A petrogenetic study of anorogenic felsic magmatism in the Cretaceous orogenic ring complex, Namibia: Evidence for mixing of crust and mantle-derived components. – *Lithos*, 54/1, 1–22. doi: 10.1016/S0024-4937(00)00033-5
- PEARCE, J.A., HARRIS, N.B.W. & TINDLE, A.G. (1984). Trace element discrimination diagrams for the tectonic interpretation of granitic rocks. – *Journal of Petrology*, 25/4, 956–983.
- PECCERILLO, A. & TAYLOR, S.R. (1976). Geochemistry of Eocene calc-alkaline rocks from Kastamonu area – Northern Turkey. – *Contributions to Mineralogy and Petrology*, 58, 63–81.
- PEI, X.Z., ZHANG, W.J. & WANG, T. (1995). Geological features and tectonic evolution of the North Qinling Mountains orogenic belt. (in Chinese, with an English Abstract). – *Northwestern Geology*, 16/4, 8–12.
- PITCHER, W.S. (1982). Granite type and tectonic environment. – *Mountain Building Processes*. – Academic Press, London, 19–40.
- QORBANI, E., BIANCHI, I. & BOKELMANN, G. (2015). Slab detachment under the eastern alps seen by seismic anisotropy. – *Earth and Planetary Science Letters*, 409, 96–108. doi: 10.1016/j.epsl.2014.10.049
- REN, S.L. (2013). Metamorphic deformation analysis of the Funiushan tectonic belt, Qinling. – Hefei University of Technology Press.
- REN, S.L., LIU, G.T. & SONG, C.Z. (2016). Deformation and metamorphic characteristics of amphiboles in the Luonan-Luanchuan fault belt of the Qinling Orogen and its significance. (in Chinese, with an English Abstract). – *Acta Petrologica Sinica*, 32/3, 775–786.
- ROBERTS, M.P. & CLEMENS, J.D. (1993). Origin of high-potassium, calc-alkaline, I-type granitoids. – *Geology*, 21, 825–828. doi: 10.1130/0091-7613(1993)021<825:OOHPTA>3E2.3.CO;2
- RUDNICK, R.L. & GAO, S. (2003). Composition of the continental crust. In: Rudnick R. L. ed., *Treatise on Geochemistry* 3. – Elsevier, Amsterdam, 1–46. doi: 10.1016/B0-08-043751-6/03016-4
- SISSON, T., RATAJESKI, K., HANKINS, W. & GLAZNER, A. (2005). Voluminous granitic magmas from common basaltic sources. – *Contrib. Miner. Petrol.*, 148, 635–661. doi: 10.1007/s00410-004-0632-9
- SONG, C.Z., LIU, G.S. & NIU, M.L. (2002). Cenozoic structures and dynamics on the northern margin of the Qinling-Dabie orogenic belt. (in Chinese, with an English Abstract). – *Geological Bulletin of China*, 21/9, 530–535.
- SONG, C.Z., ZHANG, G.W. & NIU, M.L. (2006). Oblique collision and convergence factor on the northern margin of the Qinling orogenic belt. (in Chinese, with an English Abstract). – *Geology in China*, 33/1, 48–55.
- SUN, S.S. & MCDONOUGH, W.F. (1989). Chemical isotopic systematics of oceanic basalts: Implications for mantle composition and processes. – *Magmatism in the Ocean Basins*. – Geological Society of London Special Publication, 42/1, 313–345. doi: 10.1144/GSL.SP.1989.042.01.19
- SYLVESTER, P.J. (1998). Post-collisional strongly peraluminous granites. – *Lithos*, 45, 29–44. doi: 10.1016/S0024-4937(98)00024-3
- TURNER, S., SANDIFORD, M. & FODEN, J. (1992). Some geodynamic and compositional constraints on “Postorogenic” magmatism. – *Geology*, 20/10, 931.
- WANG, J.G. & LU, X.X. (1988). The petrological features of Funiushan granite. (in Chinese, with an English Abstract). – *Geology of Henan*, 6/3, 35–40.
- WANG, J.Y., REN, S.L. & LI, J.H. (2017). Study on Deformation of Shirensan Block in the North Qinling. – *Acta Geologica Sinica – English Edition*, 91/1, 351–352.
- WANG, J.Y., REN, S.L., JIANG, D.Z., DONG, S.W., LI, J.H., LI, L.M., SONG, C.Z., HAN, H. & LI, Z.Q. (2019). New Zircon U-Pb Ages of the Shirensan Gneiss, North Qinling and Their Geological Implications. – *Acta Geologica Sinica – English Edition*, 93/1, 238–240. doi: 10.1111/1755-6724.13792
- WHALEN, J.B., CURRIE, K.L. & CHAPPELL, B.W. (1987). A-type granites: geochemical characteristics, discrimination and petrogenesis. – *Contributions to Mineralogy and Petrology*, 95/4, 407–419. doi: 10.1007/BF00402202
- WU, A.M., MARTARELLI, L., MA, R., WANG, H., YANG, H.F. & BU, H. (2018). Common and different features of Chinese and Italian hydrogeological mapping guidelines. – *Geologia Croatica*, 71/2, 105–111. doi: 10.4154/gc.2018.07
- XU, Z.Q., LI, Y. & LIANG, F.H. (2015). A connection between of the Paleo-Tethys suture zone in the Taihua group on the southern margin of the North China craton: further insights from U-Pb ages and Hf isotope compositions of zircons. – *Mineral. Petrol.*, 97, 43–59.
- XU, Z.Q., LI, Y.L. & TANG, Y.Q. (1990). The formation of the Qinling Mountain China as the backbone of China, convergence, collision and intracontinental subduction – in Chinese, with an English Abstract. – *Bulletin of the Chinese Academy of Geological Sciences*, 20/1, 130–132.
- ZHANG, G.W., DONG, Y.P. & YAO, A.P. (1997). The crustal compositions, structures and tectonic evolution of the Qinling orogenic belt – in Chinese, with an English Abstract. – *Geology of Shanxi*, 15/2, 1–14.
- ZHANG, Z.W. & LI, S.M. (1998). Sm-Nd and Rb-Sr ages of the Archean Taihua Group metamorphic rocks in the Xiong'er shan region, Western Henan province. – In: CHENG, Y.Q. (Ed.): *Precambrian Geological Research Papers of the North China Platform*. Geological Publishing House, Beijing, 123–132.
- ZHANG, G.W., ZHANG, B.R., YUAN, X.C. & XIAO, Q.H. (2001). Qinling Orogenic Belt and Continental Dynamics (in Chinese, with an English Abstract). – *Sci. Press*, Beijing, 1–86.